Materials Letters 252 (2019) 239–243

Contents lists available at ScienceDirect

Materials Letters

journal homepage: www.elsevier.com/locate/mlblue

Light absorption properties of mesoporous barium hexaferrite, $BaFe_{12}O_{19}$

Alan Bañuelos-Frías [a], Gerardo Martínez-Guajardo [b], Leo Alvarado-Perea [a,b], Lázaro Canizalez-Dávalos [b], Facundo Ruiz [c], Claudia Valero-Luna [a,*]

[a] Unidad Académica de Ingeniería Eléctrica, Universidad Autónoma de Zacatecas, Zac 98000, Mexico
[b] Unidad Académica de Ciencias Químicas, Universidad Autónoma de Zacatecas, Zac 98160, Mexico
[c] Facultad de Ciencias, Universidad Autónoma de San Luis Potosí, S.L.P 78290, Mexico

ARTICLE INFO

Article history:
Received 16 March 2019
Received in revised form 18 May 2019
Accepted 29 May 2019
Available online 30 May 2019

Keywords:
Bandgap
Barium hexaferrite
Kubelka-Munk method

ABSTRACT

Light absorption properties are one of the most important characteristics of semiconductor materials, since it is related to particle size, electric resistance, powder density, and dielectric constant. Barium hexaferrite ($BaFe_{12}O_{19}$) particles were synthesized by ceramic and chemical co-precipitation method. Light absorption properties were studied in relation to the particle size, morphology, and surface porosity. The band gap was calculated by the Kubelka-Munk method from the obtained experimental absorption spectrum. Band gap energies of 1.82 and 1.86 eV were estimated for the particles synthesized by the ceramic method and for the co-precipitation method respectively. The results show that both synthesized $BaFe_{12}O_{19}$ samples can be effectively excited with visible light irradiation. In addition to this, due to its other good characteristics such as its magnetic properties, high resistance to corrosion, and chemical stability, make the barium hexaferrite an excellent material for diverse technological applications.

1. Introduction

There are diverse methodologies for the estimation of the band gap energy for semiconductor materials, from optical to electrochemical [1–5]. The most common method used is the diffuse reflectance method, in which the absorption spectrum of the studied material is analyzed [1,2,6]. Semiconductors are mainly used as catalysts, solar cells, lasers, Gamma ray detectors, and electronic devices due to their efficient charge transference and their photon absorption properties [7,8]. Materials as MFe_2O_4, (where, M = Ba, Zn, Fe, Co, Cu, Mn), $BiFeO_3$, $BaFe_{3-x}$, present a band gap energy of ~2 eV, therefore, are efficiently exited under visible light irradiation [9–16] and in addition, has excellent magnetic properties [16–22]. $MFe_{12}O_{19}$ (where, M = Ba, Sr, Cu, Pb) [19,23–25] magnetic properties are known to be highly dependent of the electronic configuration of the substituting cations as well as on their site preference into the structure [26–29]. Barium hexaferrite is a semiconductor material, technologically important due to its low production cost and by its multiple applications as permanent magnets, as high density recording devises, speaker components, electric motors, microwave devices, and recently as catalysts [10,11,15,16,30–32]. In addition, Barium hexaferrite possesses exceptional properties as high Curie temperature, high cohesive strength, high magnetic field anisotropy, chemical stability, and corrosive resistance [30,32,33]. The goal of this work is to synthesize the $BaFe_{12}O_{19}$ by both ceramic and chemical co-precipitation method, and then study and to compare their band gap energy as a part of their optical properties, according to the particle size, morphology, surface area, and porosity.

2. Materials and methods

For the synthesis of the $BaFe_{12}O_{19}$ by the ceramic method, a mixture of barium carbonate and iron oxide was used, then the mixture was sintered at 1473 *K*, as reported by Ataie et al [34]. On the other hand, for the synthesis by the chemical co-precipitation method, barium nitrate and iron nitrate salts were precipitated at pH = 11 and then sintered at 1173 *K*, as reported in our previous work[15].

The $BaFe_{12}O_{19}$ crystalline phase was determined by the use of an X-ray diffractometer Bruker-AXS D8 Advanced with CuK radiation ($\lambda = 1.5406$ Å). The particle size and morphology were studied by Transmission Electron Microscopy (TEM, JEOL

* Corresponding author.
E-mail address: cvalero@uaz.edu.mx (C. Valero-Luna).

https://doi.org/10.1016/j.matlet.2019.05.137
0167-577X/

JEM-1230) working at 100 kV, a Scanning Electron Microscopy (SEM, JOEL 1200) working at 120 kV and additionally, with a Malvern Zetasizer model Nano ZS. The surface area and pore size were determined by the use of a surface analyzer Brunauer-Emmett-Teller (BET) Bel Sorp mini II/Bel Japan INC. The band gap energy was estimated from the measurements made with an Ocean Optics 4000-UV-VIS spectrophotometer.

3. Results and discussion

The X-ray diffraction pattern of the $BaFe_{12}O_{19}$ for both synthesis methods is shown in (Fig. 1). The characteristic diffraction peaks corresponding to the (*hkl*) planes and can be straightforward indexed in accordance to the card number JCPDS 96-100-8842. It can be seen that the characteristic peaks corresponding to the $BaFe_{12}O_{19}$ synthesized by the ceramic method are higher than the peaks of the sample synthesized by the co-precipitation method, thus indicating a larger particle size of the ceramic method sample, this can be confirmed by the particle size distribution of the $BaFe_{12}O_{19}$ as shown in (Fig. 2b and g). The average particle size was about 825 and 225 nm, for the sample synthesized by the ceramic and chemical co-precipitation method respectively.

The morphology of the $BaFe_{12}O_{19}$ particles synthesized by both methods is shown in (Fig. 2d, e, i, j), they show an undefined particle morphology with high agglomeration rate. This noticeable size variation can be attributed to the synthesis method, since higher temperatures will provoke more agglomeration and then resulting in larger particle size in the bulk.

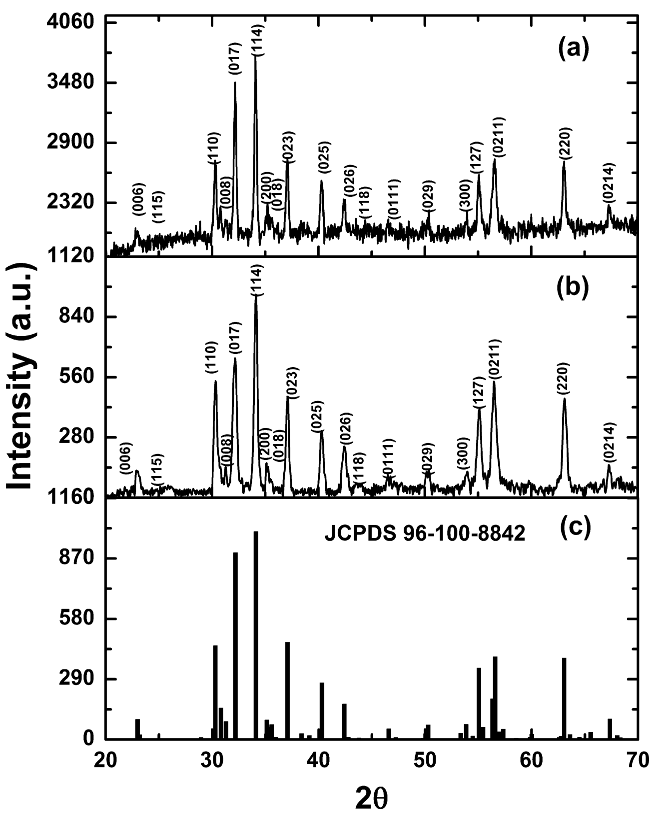

Fig. 1. XRD pattern of $BaFe_{12}O_{19}$ a) $BaFe_{12}O_{19}$ synthesized by ceramic method at 1473 K by 2 h, b) $BaFe_{12}O_{19}$ synthesized by co-precipitation method at 1173 K by 4 h and c) diffraction pattern card number JCPDS 96-100-8842.

The curves corresponding to the obtained distribution of the adsorption/desorption isotherms of $BaFe_{12}O_{19}$ particles for both synthesis methods are shown in (Fig. 2c and h). From the adsorption/desorption isotherms it can be determined that both synthesis methods produce mesoporous materials, which can be beneficial for diverse processes such as adsorption and catalysis, due to the particle surface area, as well for the solar cell production. Pore size distribution goes from 2 to 50 nm and this is attributed to defects in the particles, as it is shown in (Fig. 2d, e, i, and j). The porosity type is very specific and representative depending of the synthesis method. On the other hand, large pore sizes may result from the gaps between the agglomerated particles, while smaller pore sizes can be the result of defects generated by fractures in the particles during the cooling process.

The surface area, S_{BET}, was estimated to be around 7.1249 m^2/g and 2.0622 m^2/g for the samples synthesized by the chemical co-precipitation and ceramic method respectively, and it can be noticed that the surface area decreases as the particle size increases depending on the synthesis method.

For this work, the diffuse reflectance method was used in order to estimate the absorption edge and then the band gap energy. The estimated absorption edge for the $BaFe_{12}O_{19}$ powders was 715 and 699 nm, for particles obtained by the ceramic and for the chemical co-precipitation method respectively, as shown in (Fig. 3a). Both absorption edges comprise the visible light region and are denoted by the slope change in the absorbance spectrum, showing an excitation from the valence to the conduction band, the separation of these energetic bands is the band gap. For this reason, while studying semiconductor materials band gap it is possible to observe change in coloration depending on the particle size. Concerning to this, the ceramic method synthesis produces black powders, while the co-precipitation method yields dark brown powders respectively, with a bad gap of 1.82 and 1.86 eV without take into account the electronic transitions 1.91 and 1.97 eV considering the direct allowed transitions and finally 1.72 and 1.77 eV for the indirect transitions as it is shown in (Fig. 3b–d). In addition, the effect on the band gap of the Ba^{+2}/Fe^{+3} ratio, time and calcination temperature was also studied for the synthesis carried out by the co-precipitation method. a) 1/6.4 at 1123 K for 3 h b) 1/64 at 1173 K for 3 h c) 1/6.697 at 1173 K for 4 h and d) 1/12 at 1173 K for 4 h. The obtained Band gap were a) 1.82, b) 1.81, c) 1.83 and d) 1.79 eV, without considering the electronic transitions. However, in these reactions a mixture of phases was produced, including hematite, which is unstable in photocatalytic reactions.

In this study it was found that the sample with larger particles present a lower band gap than the sample with smaller particle size, which favors the electron transference while applying an external field. This in accordance to the study of Pattanayak et al, who observed a decrease in the electric resistance of the $BaFe_{12}O_{19}$ by decreasing the particle size [35]. The ability to absorb visible light, is one of the greatest attributes of these materials since diverse scientific research fields requires semiconductor that can be excited with the minimal possible energy amount [11,12,15,17].

4. Conclusions

Mesoporous $BaFe_{12}O_{19}$ particles were synthesized by both ceramic and chemical co-precipitation method. $BaFe_{12}O_{19}$ synthesized by the ceramic method presented a lower band gap energy (1.82 eV) than the sample synthesized by the co-precipitation method (1.86 eV), this despite the fact that the particle size of sample obtained by the ceramic method is larger (715 and 699 nm), with a larger surface area for particles

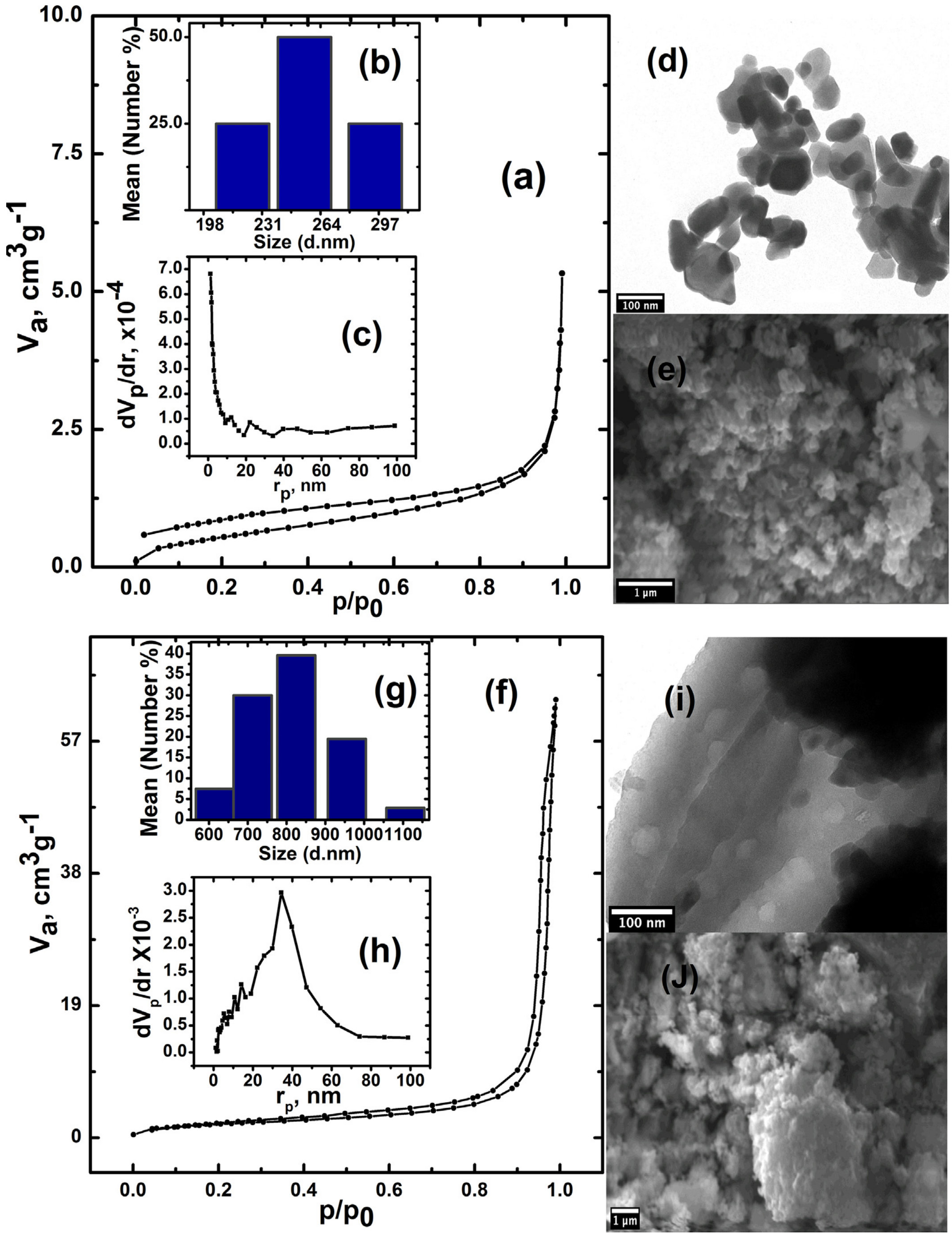

Fig. 2. (a and f) Adsorption/desorption isotherm, (b and g) particle size distribution, (c and h) pore size distribution, (d and i) TEM micrography, (e and j) SEM micrography of $BaFe_{12}O_{19}$ synthesized by co-precipitation method and ceramic method respectively.

synthesized by the co-precipitation method. Light absorption properties can be modified by variations of the synthesis method, by changing the particle size and morphology or by means of a surface functionalization. Since, these materials can be excited under visible light irradiation, and in addition to other several remarkable attributes such as low production cost, magnetic properties, high corrosion resistance and chemical stability makes $BaFe_{12}O_{19}$ an excellent material for diverse technological applications. For example, in photocatalysis, where it can be used for mineralization or production of organic compounds, and furthermore, because its magnetic properties can be easily removed from the reaction mixture.

Declaration of Competing Interest

None.

Acknowledgment

This work was supported by NPTC-SEP grant: UAZ-PTC-229.

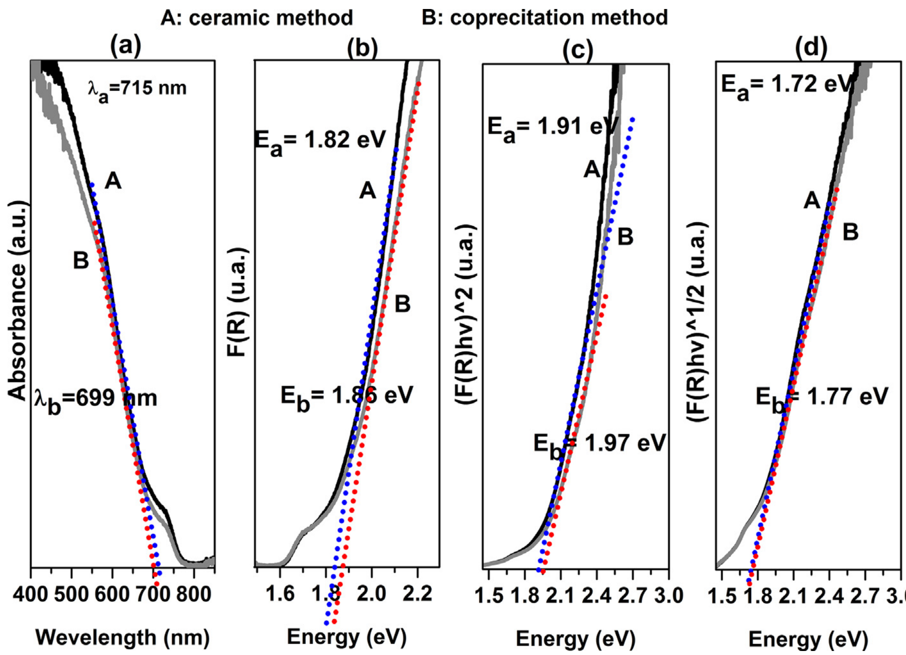

Fig. 3. (a) Edge of the absorption band, Kubelka–Munk model: (b) without considering electronic transitions, (c) direct allowed transitions, (d) indirect allowed transition of $BaFe_{12}O_{19}$ synthesized by ceramic method and co-precipitation method.

References

[1] N. Sangiorgi, L. Aversa, R. Tatti, R. Verucchi, A. Sanson, Spectrophotometric method for optical band gap and electronic transitions determination of semiconductor materials, Opt. Mater. (Amst) 64 (2017) 18–25, https://doi.org/10.1016/j.optmat.2016.11.014.

[2] N. Ghobadi, Band gap determination using absorption spectrum fitting procedure, Int. Nano Lett. 3 (2013) 2, https://doi.org/10.1186/2228-5326-3-2.

[3] R.V. Gamernyk, Y.P. Gnatenko, P.M. Bukivskij, P.A. Skubenko, V.Y. Slivka, Optical and photoelectric spectroscopy of photorefractive Sn 2P2S6 crystals, J. Phys. Condens. Matter. 18 (2006) 5323–5331, https://doi.org/10.1088/0953-8984/18/23/006.

[4] V. Srikant, D.R. Clarke, On the optical band gap of zinc oxide, J. Appl. Phys. 83 (1998) 5447–5451, https://doi.org/10.1063/1.367375.

[5] M.L. Gross, M.A. Hickner, Using cyclic voltammetry to measure bandgap modulation of functionalized carbon nanotubes, Electrochem. Solid-State Lett. 13 (2010) K5, https://doi.org/10.1149/1.3264094.

[6] A. Sobhani, M. Salavati-Niasari, Synthesis and characterization of FeSe2 nanoparticles and FeSe2/FeO(OH) nanocomposites by hydrothermal method, J. Alloys Compd. 625 (2015) 26–33, https://doi.org/10.1016/j.jallcom.2014.11.079.

[7] R. Sharma, S. Bansal, S. Singhal, Tailoring the photo-Fenton activity of spinel ferrites (MFe2O4) by incorporating different cations (M = Cu, Zn, Ni and Co) in the structure, R. Soc. Chem. 5 (2015) 6006–6018, https://doi.org/10.1039/c4ra13692f.

[8] E. Fefer, Y. Shapira, I. Balberg, Direct determination of the band-gap states in hydrogenated amorphous silicon using surface photovoltage spectroscopy, Appl. Phys. Lett. 67 (2002) 371–373, https://doi.org/10.1063/1.114632.

[9] Ö.K. Kuyumcu, Barium ferrites loaded TiO 2 usage in photocatalytic degradation of rhodamine B under visible light Görünür Işık Altında Rodamin B'nin Fotokatalitik Parçalanmasında Baryum Ferrit Yüklenmiş TiO 2 Kullanılması, J. Biol. Chem. 45 (2017) 385–393, https://doi.org/10.15671/HJBC.2018.179.

[10] D.D. Mishra, G. Tan, Visible photocatalytic degradation of methylene blue on magnetic $SrFe_{12}O_{19}$, J. Phys. Chem. Solids. 123 (2018) 157–161, https://doi.org/10.1016/j.jpcs.2018.07.018.

[11] H. Wang, Y. Xu, L. Jing, S. Huang, Y. Zhao, M. He, H. Xu, H. Li, Novel magnetic $BaFe_{12}O_{19}$/g-C3N4composites with enhanced thermocatalytic and photo-Fenton activity under visible-light, J. Alloys Compd. 710 (2017) 510–518, https://doi.org/10.1016/j.jallcom.2017.03.144.

[12] R. Dom, R. Subasri, K. Radha, P.H. Borse, Synthesis of solar active nanocrystalline ferrite, MFe_2O_4 (M: Ca, Zn, Mg) photocatalyst by microwave irradiation, Solid State Commun. 151 (2011) 470–473, https://doi.org/10.1016/j.ssc.2010.12.034.

[13] P.H. Borse, C.R. Cho, K.T. Lim, Y.J. Lee, T.E. Hong, J.S. Bae, E.D. Jeong, H.J. Kim, H. G. Kim, Synthesis of barium ferrite for visible light photocatalysis applications, J. Korean Phys. Soc. 58 (2011) 1672, https://doi.org/10.3938/jkps.58.1672.

[14] M. Hashemi, F. Mohandes, S. Ahmadian-Fard-Fini, A. Sobhani, N. Shabani-Armaki, M. Salavati-Niasari, Solvent-free preparation of copper ferrite microspheres composed of nanorods using a new coordination compound as precursor, J. Mater. Sci. Mater. Electron. 28 (2017) 11682–11688, https://doi.org/10.1007/s10854-017-6971-x.

[15] C. Valero-Luna, S.A. Palomares-Sanchéz, F. Ruíz, Catalytic activity of the barium hexaferrite with H2O2/visible light irradiation for degradation of Methylene Blue, in: Catal. Today, Elsevier B.V., 2016, pp. 110–119, https://doi.org/10.1016/j.cattod.2015.08.049.

[16] A. Abbasi, D. Ghanbari, M. Salavati-Niasari, M. Hamadanian, Photo-degradation of methylene blue: photocatalyst and magnetic investigation of Fe 2 O 3 –TiO 2 nanoparticles and nanocomposites, J. Mater. Sci. Mater. Electron. (2016), https://doi.org/10.1007/s10854-016-4361-4.

[17] P. Tiwari, R. Verma, S.N. Kane, T. Tatarchuk, F. Mazaleyrat, Effect of Zn addition on structural, magnetic properties and anti-structural modeling of magnesium-nickel nano ferrites, Mater. Chem. Phys. 229 (2019) 78–86, https://doi.org/10.1016/j.matchemphys.2019.02.030.

[18] S. Raghuvanshi, P. Tiwari, S.N. Kane, D.K. Avasthi, F. Mazaleyrat, T. Tatarchuk, I. Mironyuk, Dual control on structure and magnetic properties of Mg ferrite: role of swift heavy ion irradiation, J. Magn. Magn. Mater. 471 (2019) 521–528, https://doi.org/10.1016/j.jmmm.2018.10.004.

[19] M. Mahdiani, A. Sobhani, F. Ansari, M. Salavati-Niasari, Lead hexaferrite nanostructures: green amino acid sol–gel auto-combustion synthesis, characterization and considering magnetic property, J. Mater. Sci. Mater. Electron. 28 (2017) 17627–17634, https://doi.org/10.1007/s10854-017-7701-0.

[20] M. Mahdiani, A. Sobhani, M. Salavati-Niasari, Enhancement of magnetic, electrochemical and photocatalytic properties of lead hexaferrites with coating graphene and CNT: sol-gel auto-combustion synthesis by valine, Sep. Purif. Technol. 185 (2017) 140–148, https://doi.org/10.1016/j.seppur.2017.05.029.

[21] D. Ghanbari, M. Salavati-Niasari, M. Ghasemi-Kooch, A sonochemical method for synthesis of Fe3O4 nanoparticles and thermal stable PVA-based magnetic nanocomposite, J. Ind. Eng. Chem. (2014), https://doi.org/10.1016/j.jiec.2013.12.098.

[22] D. Ghanbari, M. Salavati-Niasari, Synthesis of urchin-like CdS-Fe3O4 nanocomposite and its application in flame retardancy of magnetic cellulose acetate, J. Ind. Eng. Chem. (2015), https://doi.org/10.1016/j.jiec.2014.09.043.

[23] F. Ansari, A. Sobhani, M. Salavati-Niasari, Sol-gel auto-combustion synthesis of PbFe12O19 using maltose as a novel reductant, RSC Adv. 4 (2014) 63946–63950, https://doi.org/10.1039/c4ra11688g.

[24] F. Ansari, A. Sobhani, M. Salavati-Niasari, PbTiO3/PbFe12O19 nanocomposites: green synthesis through an eco-friendly approach, Compos. Part B Eng. 85 (2016) 170–175, https://doi.org/10.1016/j.compositesb.2015.09.027.

[25] F. Ansari, A. Sobhani, M. Salavati-Niasari, Facile synthesis, characterization and magnetic property of CuFe12O19 nanostructures via a sol-gel auto-combustion process, J. Magn. Magn. Mater. 401 (2016) 362–369, https://doi.org/10.1016/j.jmmm.2015.10.049.

[26] M.V. Rane, D. Bahadur, A.K. Nigam, C.M. Srivastava, Mössbauer and FT-IR studies on non-stoichiometric barium hexaferrites, J. Magn. Magn. Mater. 192 (1999) 288–296, https://doi.org/10.1016/S0304-8853(98)00533-2.

[27] S.E. Jacobo, C. Domingo-Pascual, R. Rodriguez-Clemente, M.A. Blesa, Synthesis of ultrafine particles of barium ferrite by chemical coprecipitation, J. Mater. Sci. 32 (1997) 1025–1028, https://doi.org/10.1023/A:1018582423406.
[28] W.D. Townes, J.H. Fang, A.J. Perrotta, The crystal structure and refinement of ferrimagnetic barium ferrite, bafe12o19, Zeitschrift Fur Krist. – New Cryst. Struct. (1967), https://doi.org/10.1524/zkri.1967.125.125.437.
[29] R.C. Pullar, Hexagonal ferrites: a review of the synthesis, properties and applications of hexaferrite ceramics, Prog. Mater. Sci. 57 (2012) 1191–1334, https://doi.org/10.1016/j.pmatsci.2012.04.001.
[30] Z. Durmus, The effect of condensation on the morphology and magnetic properties of modified barium, Nano-Micro Lett. 3 (2011) 108–114, https://doi.org/10.5101/nml.v3i2.
[31] M.M. Hessien, M.H. Khedr, Catalytic activity and magnetic properties of barium hexaferrite prepared from barite ore, Mater. Res. Bull. 42 (2007) 1242–1250, https://doi.org/10.1016/j.materresbull.2006.10.023.
[32] S. Kanagesan, S. Jesurani, M. Sivakumar, C. Thirupathi, T. Kalaivani, Effect of microwave calcinations on barium hexaferrite synthesized via sol-gel combustion, J. Sci. Res. 3 (2011) 451–456, https://doi.org/10.3329/jsr.v3i3.6483.
[33] M. Montazeri-Pour, A. Ataie, R. Nikkhah-Moshaie, Synthesis of nano-crystalline barium hexaferrite using a reactive co-precipitated precursor, IEEE Trans. Magn. (2008) 4239–4242, https://doi.org/10.1109/TMAG.2008.2001811.
[34] A. Ataie, The effects of different precursor milling processes on the phase evolution of nanocrystalline barium hexaferrite, Int. Conf. Adv. Mater. Nanotechnol. 1217 (2007) 6–11, https://doi.org/10.1063/1.3377891.
[35] R. Pattanayak, S. Panigrahi, T. Dash, R. Mudulisurname, D. Beherasurname, Electric transport properties study of bulk BaFe12O19 by complex impedance spectroscopy, Phys. B Condens. Matter. 474 (2015) 57–63, https://doi.org/10.1016/j.physb.2015.06.006.